On the microstructure of the charge density wave observed in La$_{1-x}$Ca$_x$MnO$_3$

J. C. Loudon[a]; S. Cox[a]; N. D. Mathur[a]; P. A. Midgley[a]

[a] Department of Materials Science and Metallurgy, University of Cambridge, Cambridge, CB2 3QZ, UK

PLEASE SCROLL DOWN FOR ARTICLE

Taylor & Francis
Taylor & Francis Group

On the microstructure of the charge density wave observed in $La_{1-x}Ca_xMnO_3$

J. C. LOUDON*, S. COX , N. D. MATHUR and P. A. MIDGLEY

Department of Materials Science and Metallurgy, University of Cambridge,
Pembroke Street, Cambridge, CB2 3QZ, UK

We have used low temperature (90 K) transmission electron microscopy to investigate the 'charge ordering' modulation in the mixed valent manganite, $La_{1-x}Ca_xMnO_3$. It has been stated that Mn^{3+} and Mn^{4+} ions order at low temperature to produce a structural modulation composed of supercells whose size is an integer multiple of the unmodulated unit cell. Here, we use convergent beam electron diffraction to show that the periodicity of the modulation need not be an integer multiple of the undistorted cell, even on the smallest scales. We therefore suggest that this modulation is a charge density wave with a uniform periodicity. We show that the modulation wavevector lies close to the **a*** axis of the crystal but need not be exactly collinear. A typical grain of size 0.5 μm in $La_{0.48}Ca_{0.52}MnO_3$ had a wavevector which varied on a scale of tens of nanometres with an average of $\langle \mathbf{q} \rangle = 0.450\mathbf{a^*}$ and a standard deviation $\Delta q = 0.004\,a^*$ in its magnitude and $\Delta\theta = 0.56°$ in its direction at 90 K. The magnitude of the wavevector in this composition fell by 20% as the temperature was increased from 90 K to room temperature. This change occurred by nucleation and growth. Although weak, the modulation was still present at room temperature, some 30 K above the 'charge ordering temperature'.

1. Introduction

The study of mixed-valent manganites such as $La_{1-x}Ca_xMnO_3$ has aroused much interest because these compounds display an unusual coexistence of charge-ordered antiferromagnetic and metallic ferromagnetic phases [1]. Charge ordering has been described as a localization of Mn^{3+} and Mn^{4+} ions which occurs as the specimen is cooled below the charge ordering transition temperature indicated by a sudden upturn in the resistivity as the sample is cooled [2]. This transition is accompanied by the appearance of superlattice reflections in X-ray, neutron and electron diffraction experiments indicating that the crystal structure has become modulated [2, 3]. The resistivity anomaly occurs at the same temperature at which the magnetic

---

*Corresponding author. Email: james.loudon@physics.org

susceptibility shows a sudden downturn on cooling and therefore this phase has been described as antiferromagnetic and charge ordered [2].

In his review of modulated structures, Bak [4] distinguishes three types of modulation. The first is a 'commensurate' structure where the periodicity of the modulation is related to the periodicity of the undistorted lattice by a rational fraction. The second is an 'incommensurate' structure where the periodicity of the modulation is unrelated to that of the undistorted lattice. Finally there is a 'chaotic' structure where the modulation has no long range periodicity but is composed of a random mixture of small subunits of varying lengths, the length of each subunit being an integer multiple of the size of the undistorted unit cell. The appearance of a diffraction pattern from such a structure is treated mathematically by Shao [5]. Notice that these definitions are different to those normally used when referring to the 'charge ordering' modulation observed in the manganites where 'commensurate' describes a modulation whose periodicity is an integer (rather than a rational) multiple of the undistorted unit cell and 'incommensurate' describes any modulation which is not commensurate [3, 6].

It is well known that when $x > 0.5$, the periodicity of the modulation is primarily determined by the calcium doping concentration and the modulation wavevector $\mathbf{q}$, expressed as a fraction of the reciprocal lattice vector a^*, broadly follows the relationship $q = 1 - x$ where $\mathbf{q}$ is approximately collinear with the $\mathbf{a}^*$ direction (labelling the unmodulated structure as orthorhombic P*nma*) [3, 7]. Thus, the modulation in $La_{1/2}Ca_{1/2}MnO_3$ shows a doubling of the undistorted cell, $La_{1/3}Ca_{2/3}MnO_3$ shows a tripling and $La_{1/4}Ca_{3/4}MnO_3$ shows a quadrupling [6]. This immediately begs the question of what happens in-between these compositions. Few authors investigate compositions that do not give integer period modulations but it is generally accepted that the modulation is 'chaotic' in the sense defined by Bak [4]. Mori *et al.* [6] state that '. . . such cases show that charge ordering appears as a proper mixture of the two adjacent distinct commensurate configurations according to the lever rule. For example, a sample with $x = 5/8$, between $1/2$ and $2/3$ . . . is found to exhibit a fine mixture of 25% $2a$ and 75% $3a$. The minority $2a$ configuration . . . appears as incoherent stacking-fault defects in the otherwise perfect $3a$ configuration'. In this paper we show that far from forming a 'chaotic' structure, the modulation observed in $La_{1-x}Ca_xMnO_3$ has a uniform periodicity even on the smallest scales.

2. Mathematical treatment of a structural modulation

We briefly describe the appearance of a diffraction pattern from a sinusoidally modulated crystal structure using the derivation given by Giacovazzo *et al.* [8]. Although the modulation observed in the manganites may not be sinusoidal, it has a uniform periodicity on an atomic scale and this treatment represents the principal Fourier component of the modulation. As such, we use it as a guide to interpreting diffraction patterns taken from modulated manganite crystals.

In a perfect, unmodulated crystal, the position of a unit cell is defined by the lattice vector $\mathbf{r_u} = u\mathbf{a} + v\mathbf{b} + w\mathbf{c}$ and the position of the jth atom within the unit cell is given by $\mathbf{R}_j$. Thus, a given atom is located by the position of the unit cell and the position of the atom within the unit cell thus:

$$\mathbf{r}_{\mathbf{u},j} = \mathbf{R}_j + \mathbf{r_u}. \tag{1}$$

We consider deforming the lattice with a sinusoidal modulation of amplitude, $\mathbf{A}_j$, phase, φ_j, and wavevector, $\mathbf{q}$. The positions of the atoms are now given by

$$\mathbf{r}_{\mathbf{u},j} = \mathbf{R}_j + \mathbf{r_u} + \mathbf{A}_j \sin(2\pi\mathbf{q}.(\mathbf{R}_j + \mathbf{r_u}) - \phi_j). \qquad (2)$$

A calculation of the structure factors that arise from such a modulated structure shows that diffraction peaks occur at $\mathbf{H}' = h\mathbf{a}^* + k\mathbf{b}^* + l\mathbf{c}^* + m\mathbf{q}$ (where h, k, l, m are integers) and have structure factors given by

$$F_{\mathbf{H}'} = \sum_j f_j(\mathbf{H}')e^{2\pi i\mathbf{H}'.\mathbf{R}_j}e^{-2\pi i\mathbf{q}.\mathbf{R}_j}(-1)^m J_m(2\pi\mathbf{H}'.\mathbf{A}_j)e^{im\phi_j}, \qquad (3)$$

where J_m is the mth order spherical Bessel function and f_j is the scattering factor of atom j.

This analysis shows that diffraction peaks occur in the same positions as in the unmodulated structure, $\mathbf{g} \equiv h\mathbf{a}^* + k\mathbf{b}^* + l\mathbf{c}^*$. However, each of these so-called 'parent' reflections is decorated with satellite reflections which occur at integer multiples of the modulation wavevector on either side of each parent reflection, that is at $\mathbf{g} \pm m\mathbf{q}$. The intensity of the satellite reflections falls rapidly as the order, m, of the satellite reflection increases as described by equation (3).

If the modulation is transverse as predominantly occurs in the manganites (see section 4.4), $\mathbf{q}$ is perpendicular to $\mathbf{A}_j$ and if $\mathbf{q}$ is parallel to $\mathbf{a}^*$, as is broadly the case for the manganites, $\mathbf{H}'$ is parallel to $\mathbf{q}$ if k and l are 0. So for this case, no superlattice reflections should occur on the $k = l = 0$ row of a diffraction pattern. Note that this assumes that diffraction is kinematic (i.e. the incident radiation only undergoes single scattering events so that the intensity of the diffracted beams are proportional to the squared modulus of their structure factors). Electron diffraction involves multiple scattering (dynamical diffraction) so that it is necessary to tilt the specimen to diffraction conditions where multiple scattering is minimised in order to approximate the kinematic case as we have done in section 4.4 [9].

3. Experimental details

3.1. *Sample synthesis and preparation*

The samples of La$_{1-x}$Ca$_x$MnO$_3$ used in this investigation were synthesised by A. J. Williams at the Chemical Laboratory, Cambridge University. They were prepared by repeated grinding, pressing and sintering of La$_2$O$_3$, CaCO$_3$ and MnO$_2$ in stoichiometric proportions. The La$_2$O$_3$ was heated overnight prior to use in order to dehydrate it. Each sample was prepared by initially heating at 950°C for 12 hours to decarboxylate the CaCO$_3$, and then 1350°C for 12 hours. Each sample was then reground, repelleted and heated at 1350°C for 4 days; and then reground, repelleted and reheated at 1300°C for 2 days. X-ray powder diffraction confirmed the presence of a single phase. Large area ($10 \times 10\,\mu$m) energy dispersive X-ray analysis using a scanning electron microscope showed that the La/Ca ratio was constant to within the error of the measurements ($\delta x = \pm 2\,\%$). The samples were prepared for transmission electron microscopy by conventional mechanical polishing and argon ion thinning at liquid nitrogen temperatures using a Gatan Duo Mill ion thinner. Samples with compositions $x = 0.50$, 0.52, 0.58, 0.67 and 0.71 were used in this investigation.
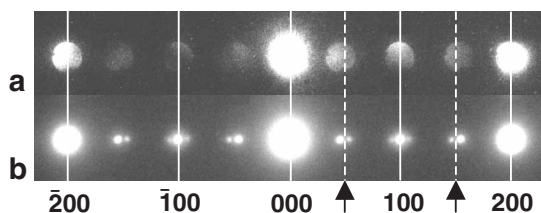
Figure 1. Diffraction patterns on different length scales. (a) A convergent beam electron diffraction (CBED) pattern from a $La_{0.48}Ca_{0.52}MnO_3$ grain at 90 K. Parent reflections are delineated by solid lines. The random mixture model predicts that $x = 1/2$ sub-units should outnumber $x = 2/3$ sub-units by a factor of 7.3 such that the latter are on average 7.8 nm apart. The CBED probe FWHM is 3.6 nm (6.7 room temperature unit cells). In all CBED patterns acquired, $q = 1/2$ (indicated by arrows and dashed lines) or $q = 1/3$ modulations are never seen and instead $q = 0.473 \pm 0.005$. (b) Diffraction pattern from the same grain taken with a selected area aperture of diameter 500 nm (as measured in the object plane). The wavevector $q = 0.468 \pm 0.003$. This matches the CBED value within experimental error.

3.2. *Transmission electron microscopy*

Transmission electron microscopy was carried out using Philips CM30 and CM300FEG electron microscopes. A Gatan liquid nitrogen-cooled specimen stage was used to cool the samples to 90 K. Images and diffraction patterns were recorded on CCD cameras and photographic plates.

4. Results

4.1. *Uniform periodicity on all length scales*

The concept that the modulation is made up of small, integer period sub-units was derived from lattice images taken using high resolution electron microscopy [7]. Such lattice images are not directly interpretable and one cannot easily assign different atomic species, let alone different ionic valencies, to the features observed in these images as is sometimes claimed. Only the periodicity of the structure can be directly interpreted and this is readily determined from fast Fourier transforms of high resolution images. When we carried out this procedure, we found that for compositions $x \neq 1/2$, 2/3, 3/4 the periodicity of the modulation remained at a non-integer multiple of a irrespective of the area of the image that was investigated.

The most rigorous test performed in this work involved using convergent beam electron diffraction [9] which allowed the periodicity of the lattice to be determined on very small length scales. This experiment was conducted at 90 K, the lowest temperature accessible with the liquid nitrogen cooled specimen stage and more than 120 K below the 'charge ordering temperature' at which anomalies occur in resistivity and magnetisation data [1]. It has been stated explicitly [6] that the charge ordering modulation should be composed of integer periods at this temperature. The composition $x = 0.52$ was chosen for this experiment as it is close to the composition $x = 0.5$ and so the modulation should be composed mostly of sub-units of size $2a$ which outnumber those of size $3a$ by a factor of 7.3 (assuming that the modulation is composed only of subunits of size $2a$ and $3a$). Thus, subunits of $3a$ should be 7.8 nm apart on average, separated by continuous runs of subunits of $2a$. If other sub-units

such as $4a$ and $5a$ are present, the average length of a continuous run of subunits of $2a$ will be even larger. Thus, diffraction patterns taken from regions of less than 7.8 nm should mostly show the periodicity $2a$ (or a wavevector $q = 1/2$).

Convergent beam electron diffraction patterns with a probe size of 3.6 nm (full width half maximum) were then taken from La$_{0.48}$Ca$_{0.52}$MnO$_3$, an example of which is shown in figure 1a. None showed a wavevector of $q = 1/2$ or $1/3$ and instead a uniform modulation of wavevector $q = 0.473 \pm 0.005$ was observed. This agrees with the wavevector $q = 0.468 \pm 0.003$ obtained from a selected area diffraction pattern taken from the same grain using an aperture of diameter 500 nm (as seen in the object plane) shown in figure 1b.

This shows that the 'charge ordering' modulation observed in La$_{1-x}$Ca$_x$MnO$_3$ does not form a 'chaotic' structure (in the sense defined by Bak [4]) but has a uniform periodicity on all lengthscales and this periodicity need not be an integer multiple of the undistorted unit cell. This result throws doubt on the concept of charge order as localised Mn^{3+} and Mn^{4+} ions as discussed in section 5.

4.2. *Variation of wavevector with doping*

It is well known that the structural modulation observed when charge ordering occurs is found to have a wavevector related to the composition by $q = 1-x$ at low temperatures [7]. Figures 2a and 2b show diffraction patterns for compositions $x = 0.52$ and 0.71 taken at 90 K. First order ($m = 1$) superlattice reflections can be clearly seen at $\mathbf{g} \pm \mathbf{q}$ and weaker, second order ($m = 2$) reflections can be seen at $\mathbf{g} \pm 2\mathbf{q}$. Figure 2c is a plot of the wavevector observed at 90 K versus composition, constructed from these and other diffraction patterns. It can be seen that the wavevector appears to follow the general trend $q = 1-x$ but there are significant departures from this relationship. It should be noted that all but one of the points show wavevectors which are smaller than the wavevector predicted by the formula $q = 1-x$ possibly suggesting that the wavevector tends towards the value given by $1-x$ as the temperature is lowered but the transition may be inhibited and the wavevector may remain frozen in a non-equilibrium state as discussed in section 4.8.

4.3. *Twinning*

Sharp and strong reflections with wavevector $\mathbf{q}$ were observed at 90 K at all compositions investigated between $0.5 \leq x \leq 0.71$. In this work and that of other authors [11], $\mathbf{q}$ is found to be nearly collinear with the $\mathbf{a^*}$ axis of the crystal. The diffraction pattern in figure 3a appears to show the modulation wavevector parallel to both the $\mathbf{a^*}$ and $\mathbf{c^*}$ directions but as shown by the dark field images in (b) and (c), this is caused by perpendicular twins contributing to the diffraction pattern.

Several features of the twins are immediately apparent. The first is the speckled contrast observed in the dark field image. This appears to indicate that some regions of the crystal are charge ordered (and appear bright) whilst others are not charge ordered (and appear dark). In fact it is shown in section 4.7 that at this temperature the whole area is charge ordered and the speckle probably arises from small out of plane variations of the wavevector. It can also be seen from these images that the straight sections of the twin boundaries are approximately parallel to the [101] and [$\bar{1}$01] directions as has also been observed by Chen and Cheong [12]. The twin boundaries also have large non-crystallographic curved sections indicating that the energy of the boundary is low.
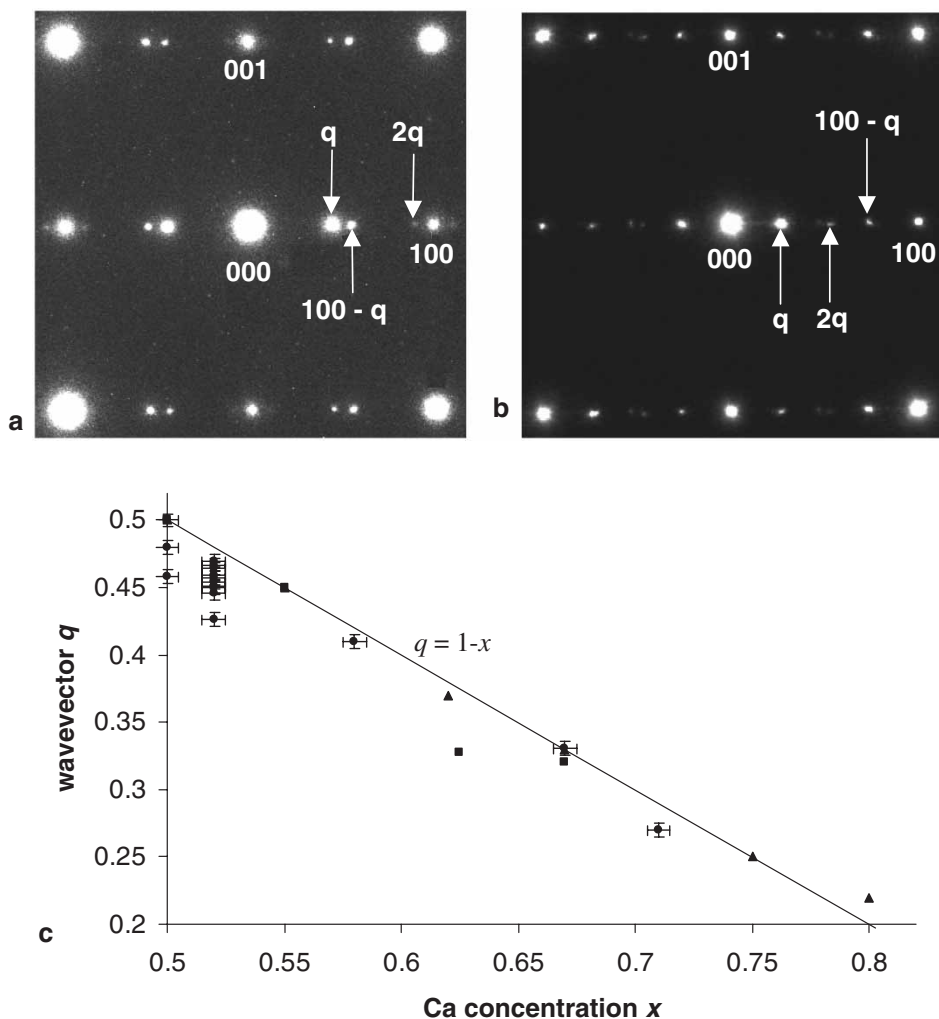
Figure 2. Wavevector at 90 K observed at different doping concentrations by electron diffraction. (a) A diffraction pattern from the [010] zone axis of $La_{0.48}Ca_{0.52}MnO_3$. Superlattice reflection can be observed at $\mathbf{g} \pm \mathbf{q}$ and $\mathbf{g} \pm 2\mathbf{q}$. (b) A similar diffraction pattern for $La_{0.29}Ca_{0.71}MnO_3$. (c) A graph of wavevector against Ca concentration. Circles with error bars are from this work, squares from Chen *et al.* [10] and triangles from Chen *et al.* [7]. All but one of the points lie below the expected value indicated by the straight line. The errors in the measurement of the wavevector were determined by measuring the wavevector at several different places in the same diffraction pattern and finding the standard error of these measurements. The error in the Ca concentration is that estimated for the macroscopic concentration. The variation in concentration from one grain to another may be greater than this.

It has been shown [11] that these twins are not caused by charge ordering and are present at room temperature. The twins are related by a 90° rotation of the **a** and **c** axes but are very difficult to distinguish parallel to the [010] zone axis at room temperature because **a** and **c** are very similar in magnitude. However, Wang *et al.* [11] point out that they can be distinguished by taking diffraction patterns parallel to
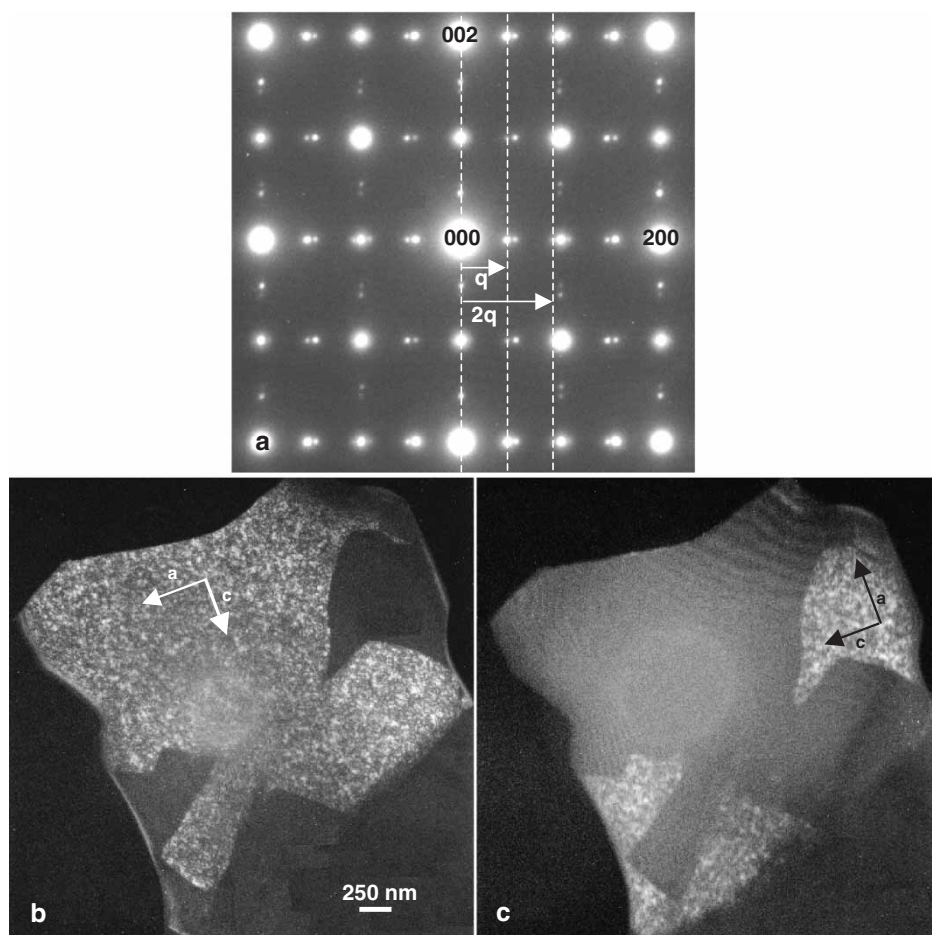
Figure 3.   Diffraction pattern and dark field images taken from La$_{0.48}$Ca$_{0.52}$MnO$_3$ at 90 K. (a) appears to show the modulation wavevector in both the **a*** and **c*** directions. However, taking dark field images from each type of reflection (at positions 002 + **q**) shown in (b) and (c) demonstrates that the pattern seen in (a) is in fact the superposition of two crystallographic twins related by a 90° rotation.

the [100] and [001] zone axes. They find that the charge ordering wavevector always lies close to **a*** and is never seen parallel to the **c*** direction.

4.4. *Transverse modulation*

When tilting the specimen away from the zone axis in order to perform dark field imaging, it was found that the superlattice reflections became very weak if the specimen was tilted about the **a**-axis to give a strong systematic row along **a*** as illustrated in figure 4. Equation (3) shows that if the amplitude of the modulation, **A**, is perpendicular to **a***, then superlattice reflections along the **a*** direction are kinematically forbidden. Since **q** is parallel to **a***, figure 4 shows that the amplitude of the modulation is approximately perpendicular to the wavevector and thus the wave has a
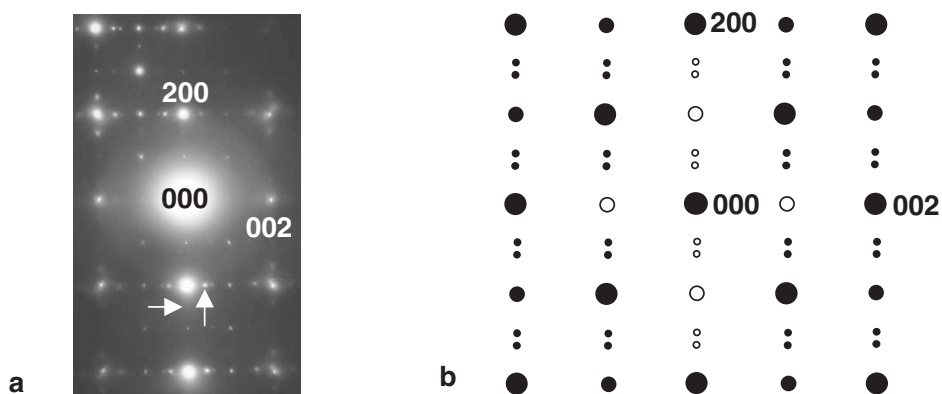
Figure 4. Transverse modulation in $La_{1-x}Ca_xMnO_3$. (a) A diffraction pattern in which the crystal has been tilted to give a strong systematic row parallel to a^* to minimise the effects of double diffraction. Superlattice reflections can be seen apparently along both a^* and c^* directions but this is in fact due to twinning (see figure 4). It can be seen that although both sets of reflections off the row have comparable intensities (see for example the reflections around 202), reflections perpendicular to the a^* row are far stronger than those along the row as shown by the white arrows. (b) Summary of this information. Filled circles show kinematically allowed reflections and empty circles show kinematically forbidden reflections.

predominantly transverse nature. This observation has also been made by other authors using neutron and X-ray diffraction [3].

4.5. *Rotation of the wavevector*

Although the wavevector **q** usually lies very close to the **a*** direction, significant departures have been observed. The largest departure observed in this investigation was in $La_{0.29}Ca_{0.71}MnO_3$ as shown by the diffraction pattern in the inset of figure 5. It shows that **q** is rotated about the [010] axis by an angle of $1.9°$ from **a*** towards the **c*** direction. This can also be seen in the high resolution image from the same area if viewed at a glancing angle parallel to the superlattice rows. The image also demonstrates that the rotation is intrinsic to the modulation and not caused by faulting. This also throws doubt on the standard models for charge ordering which predict that the wavevector is strictly parallel to **a*** [6] as discussed in section 5.

4.6. *Variation of the wavevector with temperature*

Figure 6a shows the variation with temperature of the wavevector observed in $La_{0.48}Ca_{0.52}MnO_3$. Other authors have remarked on the large reduction in wavevector that occurs in the manganites when compared with other charge density wave systems [10]. Surprisingly, the modulation is still present at room temperature (293 K) as shown in figure 6b, well above the charge ordering transition temperature of 230 K obtained from resistivity and magnetisation measurements performed on this particular sample [13], although the amplitude of the modulation is greatly reduced.

It can also be seen that the superlattice reflections are broader at room temperature than at 90 K. Estimates of the correlation length of the charge ordered regions can be found by finding the full width half maximum of the charge order reflections
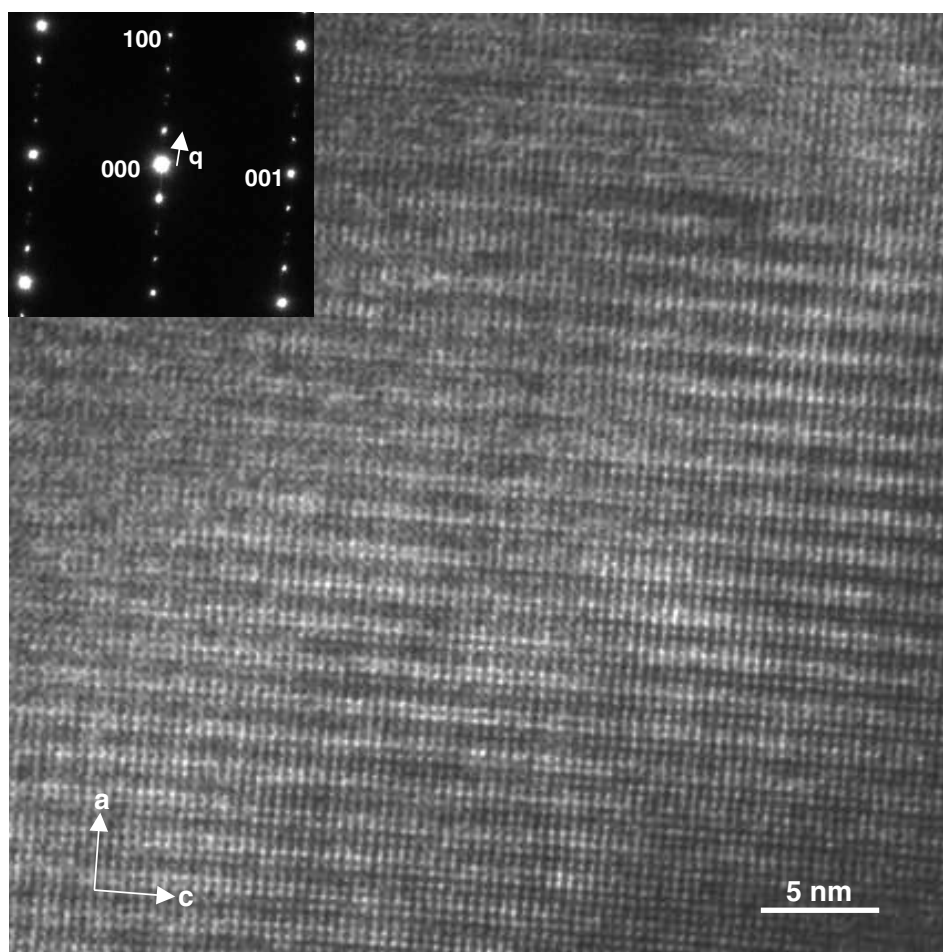
Figure 5. High-resolution image taken from $La_{0.29}Ca_{0.71}MnO_3$ at $90\,K$ parallel to the [010] zone axis. The inset shows a diffraction pattern from the same region. The wavevector $q = 0.27$ and is rotated $1.9°$ from the $a*$ direction. Note that 2nd order superlattice reflections can be seen at $2q$.

and finding the reciprocal of this quantity. This analysis showed that the correlation length at $90\,K$ is $34 \pm 7\,nm$ and at $297\,K$ it is $3.6 \pm 0.2\,nm$.

Surprisingly, dark field images discussed in section 4.7 showed that the correlation length does not reflect the sizes of charge ordered clusters within an unmodulated background. Instead, the entire grain appears to be charge ordered and the correlation length indicates the distance over which the wavevector remains constant.

In charge density wave systems and other systems that show modulated structures, the wavevector q is frequently seen to change in discrete jumps as a function of temperature (called a 'staircase'). The conventional explanation for this is based on the results of the Frenkel–Kontorova model which predicts that the wavevector locks into plateaus of stability which occur when q is a rational fraction of the reciprocal lattice vector [4]. As far as the system studied in this investigation is
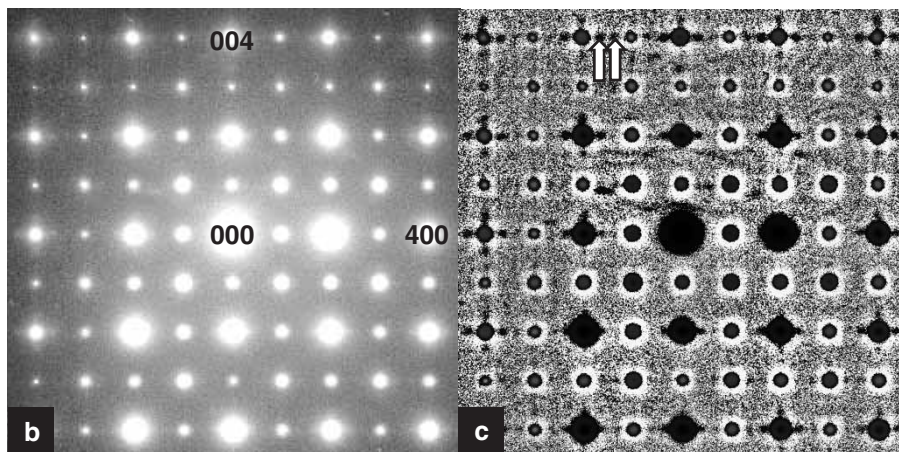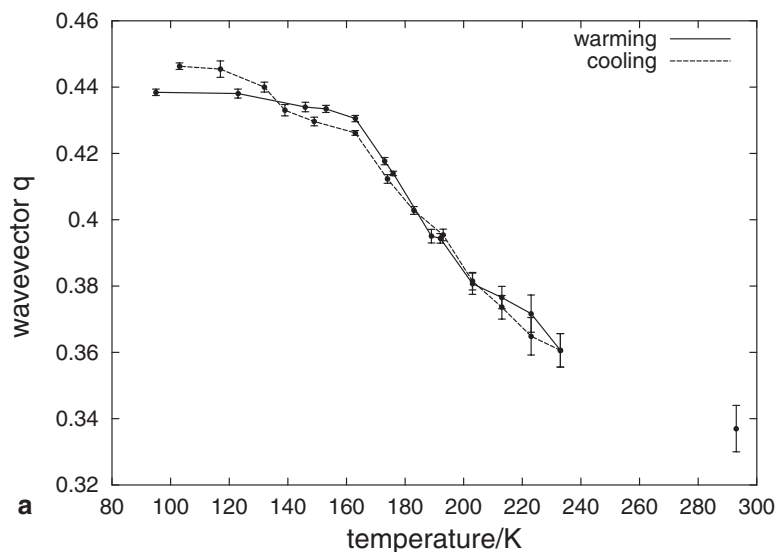
Figure 6. Variation of wavevector with temperature in $La_{0.48}Ca_{0.52}MnO_3$. Measurements were taken first on warming from 90 K to 240 K and then on cooling back to 90 K. The point at 293 K is from a different region of sample. The errors in the measurement of the wavevector were determined by measuring the wavevector at several different places in the same diffraction pattern and finding the standard error of these measurements. (b) A diffraction pattern from $La_{0.48}Ca_{0.52}MnO_3$ taken at room temperature. (c) The same diffraction pattern after high pass filtering to enhance the superlattice reflections (two of which are marked by arrows). The region of specimen from which this pattern was recorded was twinned as in figure 3 and so superlattice reflections can be seen in two perpendicular directions.

concerned, this does not appear to be the explanation for the structure of the $q(T)$ diagram shown in figure 6a.

In the warming curve, it appears that the wavevector has locked-in at low temperatures and has the value $q = 0.438 \pm 0.001$. The nearest rational fraction value to this is $7/16 = 0.4375$.

When cooled again, the modulation no longer stabilises at $q = 0.438 \pm 0.001$ but goes straight through this value, reaching $q = 0.446 \pm 0.001$ (for which the nearest rational fraction is $17/38 = 0.447$). We do not expect a plateau which was formerly stable to become unstable during thermal cycling. We conclude therefore that the graph of $q(T)$ does not follow a staircase structure whereby the wavevector locks into plateaus of stability as the temperature is changed. Instead, we believe that the modulation wavevector tends towards $q = 1 - x$ via a nucleation and growth process as the temperature falls but becomes pinned at non-equilibrium wavevectors giving rise to apparent plateaus. Pinning of the wavevector at non-equilibrium values also explains why different regions of the same sample show different wavevectors as shown in figure 2c. This explanation is consistent with the fact that changes in wavevector occur by a nucleation and growth process as discussed in section 4.8.

4.7. *Spatial variations of the wavevector*

A very accurate way to measure spatial variations in the wavevector is to take dark field images which include not only the wavevector **q** but also the conjugate wavevector **g** – **q** in the objective aperture (see figure 7a). Interference fringes are then seen with a wavevector $\varepsilon = \mathbf{g} - 2\mathbf{q}$. It should be noted that this procedure is often performed accidentally if the two superlattice reflections lie close to one another and the
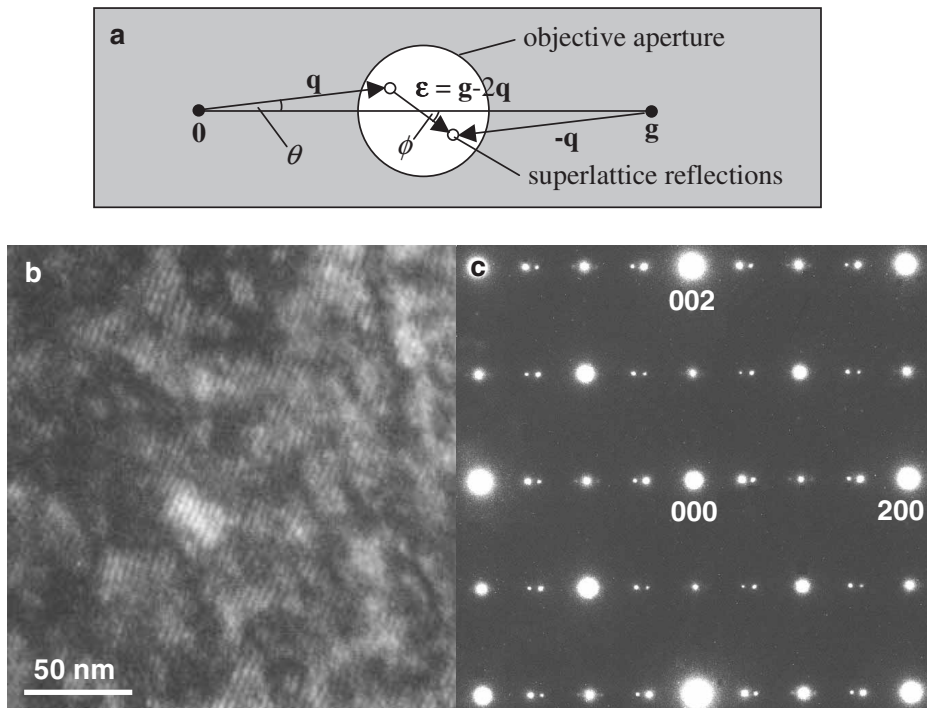
Figure 7.   Spatial variations of the wavevector **q** in La$_{0.48}$Ca$_{0.52}$MnO$_3$ at 90 K. (a) The definition of the angles in the diffraction pattern and the placement of the objective aperture. (b) A region from the dark field image with fringes spaced by $1/(g-2q)$. Notice the changes in magnitude and direction of the wavevector that occur on a scale of tens of nanometres. (c) A diffraction pattern from the same area.

resulting interference fringes have been mistaken for soliton arrays [14]. This method is very sensitive to small changes in the angle that the wavevector makes with the parent reflections and any changes in the magnitude of **q**. It can be seen from the figure that the closer q approaches $q = 1/2$, the higher this sensitivity becomes.

Experimentally one observes the wavelength of the interference fringes $\Lambda = 1/\varepsilon$ and the angle φ as defined in figure 7. These are related to q and θ via:

$$q = \frac{1}{2}\sqrt{g^2 + \varepsilon^2 - 2\varepsilon g \cos \phi} \qquad (4)$$

$$\tan \theta = \frac{\varepsilon \sin \phi}{g - \varepsilon \cos \phi}. \qquad (5)$$

Figure 7b shows a region from a grain of size about $0.5\,\mu m$ in $La_{0.48}Ca_{0.52}MnO_3$. Statistics were gathered from the whole grain using images like figure 7b, by taking fast Fourier transforms from 80 regions of size 50 nm. This gave the result that the average wavevector was $\langle q \rangle = 0.450$ and the standard deviation of q was $\Delta q = 0.004$. For this sample the average wavevector was parallel to the **a*** axis and varied about this mean orientation with an angular standard deviation of $\Delta \theta = 0.56°$.

The most noticeable feature of the dark field images is that they have dark and bright patches of size 10–50 nm. It may be thought at first that the bright patches refer to the modulated structure and the dark patches are areas which are not modulated but this proved not to be the case. Convergent beam electron diffraction patterns with a probe size of 4 nm were taken from 20 regions and although the black patches can be as large as 50 nm in size, the diffraction patterns always showed the modulation. Taking dark field images and tilting the specimen by about $1°$ showed that dark patches could become bright and bright patches dark as shown for $La_{0.5}Ca_{0.5}MnO_3$ in figure 8a and 8b. Given that the angle made by the modulation can vary in the *ac* plane by about $0.5°$, it seems reasonable to assume that it can also vary by a similar amount in the **b** direction. If this is the case, it explains the mottled appearance of the dark field image. Different patches have different components of the wavevector in the **b** direction and thus have slightly different orientations for exciting strong Bragg diffraction. Small tilts of the crystal excite different patches as illustrated schematically in figure 8c.

4.8. *Changes in wavevector by nucleation and growth*

In section 4.6, we postulated that the changes in wavevector take place by a nucleation and growth process. Figure 9 confirms this hypothesis by showing two large areas $(>0.1\,\mu m)$ with different wavevectors coexisting in the same crystallite of $La_{0.5}Ca_{0.5}MnO_3$ at 90 K. The interface between these two areas is marked by a dashed line and we postulate that if the sample were further cooled, this interface would move in the direction shown by the arrow so that the area with wavevector $q = 0.48$ would grow at the expense of the area with wavevector $q = 0.46$ and that, if kinetics allowed, further wavevectors would nucleate and grow until the whole grain eventually had a wavevector $q = 0.5$ as given by the composition.

We notice that the area with wavevector $q = 0.48$ occurs near the edge of the grain which is normal to the wavevector. The diagrams in figure 10 illustrate why this might be. Panel (a) shows the case of a new wavevector growing within the bulk of the material. There is an energy cost associated with forming an interface between
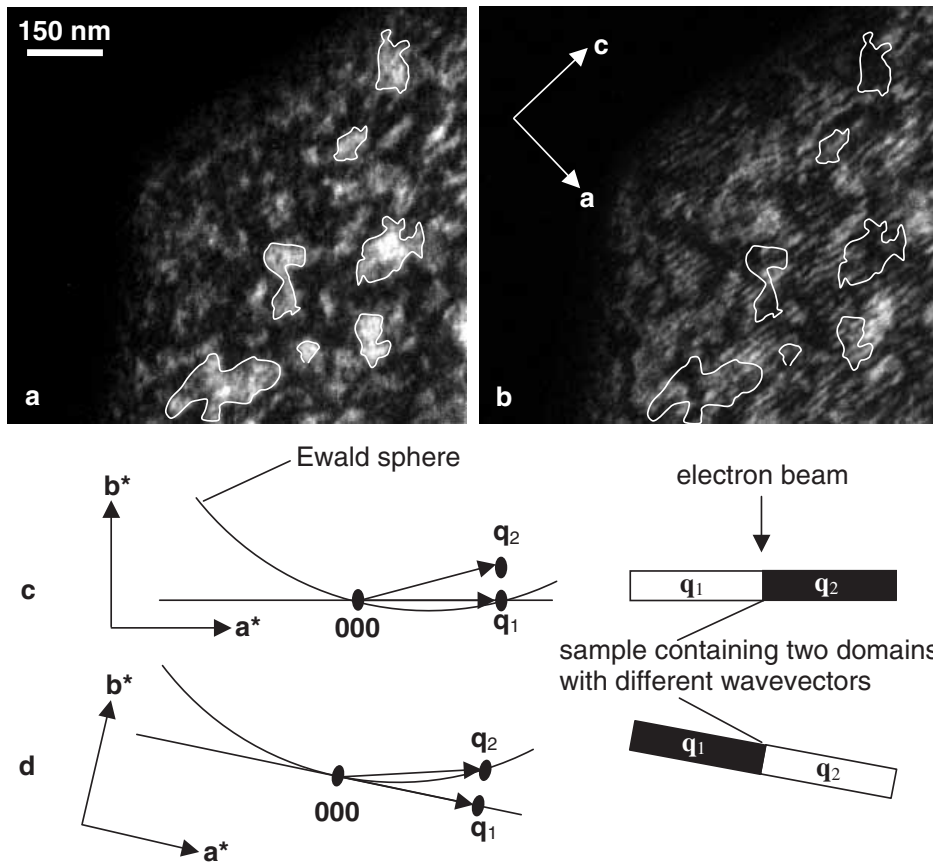
Figure 8.   Dark field images from La$_{0.5}$Ca$_{0.5}$MnO$_3$ at 90 K. (a) A dark field image taken from the $002 + \mathbf{q}$ superlattice reflection. Bright regions are outlined. (b) A dark field image from the same region using the same reflection but tilted slightly ($\sim 1°$) with respect to (a). The same regions are outlined but it can be seen that they are no longer bright. An explanation for this effect is illustrated schematically in (c) and (d). The left hand panel of (c) shows a cross section of a diffraction pattern with two domains contributing to it. One domain has a wavevector $\mathbf{q}_1$ oriented along $\mathbf{a}^*$, the other has a wavevector $\mathbf{q}_2$ with a small $\mathbf{b}^*$ component. The specimen is oriented so that the Ewald sphere intersects $\mathbf{q}_1$ and so the domain containing $\mathbf{q}_1$ is bright as illustrated in the right hand panel. In (d), the specimen is tilted slightly so that the domain containing $\mathbf{q}_2$ is bright.

the regions with different wavevector. Panel (b) shows that there is an energy saving if the new wavevector nucleates at the edge of the grain since the size of the interface is reduced. There is, however, a large mismatch between the two lattices if the interface runs parallel to the wavevector. Panel (c) shows that the minimum energy configuration is for nucleation to occur at an edge or linear defect and for the interface to be normal to the wavevector.

4.9. *Defects in the charge density wave*

Where a region with a particular wavevector meets another region with a different wavevector, there must be misfit 'dislocations' at the interface. Such dislocations are
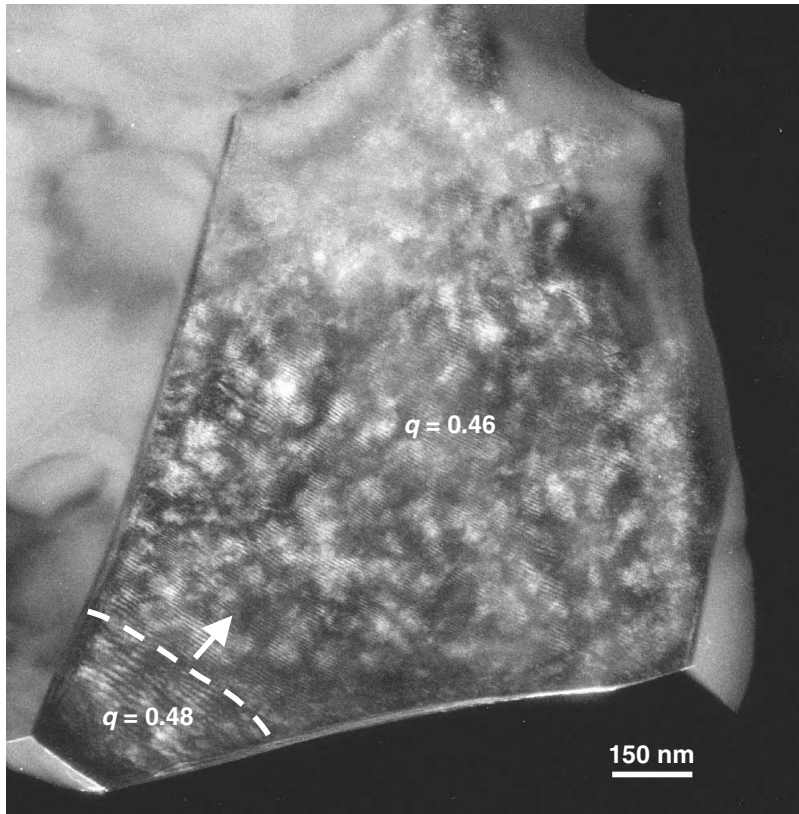
Figure 9. Coexistence of two different wavevectors in $La_{0.5}Ca_{0.5}MnO_3$ at 90 K. The bulk of the grain has a wavevector of $q = 0.46$ but a wavevector of $q = 0.48$ is observed at one edge of the grain and the interface between these two is shown by the dashed line. If the sample were further cooled, we postulate that the interface would propagate across the grain as indicated by the arrow.
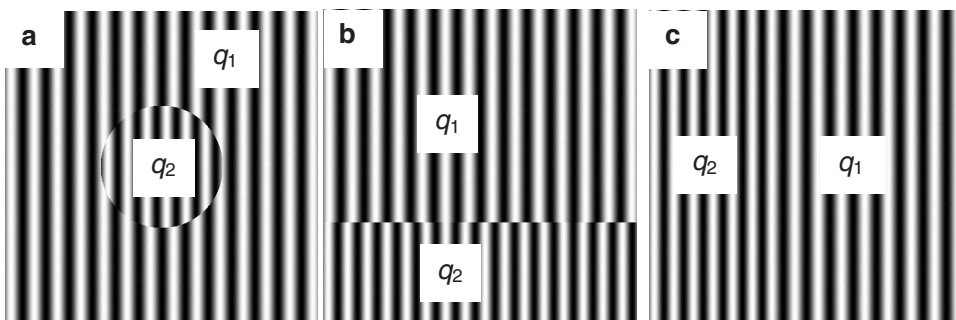
Figure 10. Schematic diagram of the nucleation of a new region with a different wavevector. The square represents a grain and the black and white lines show peaks and troughs of the modulation. (a) The new wavevector forming as a nucleus within the bulk of the grain. (b) The new wavevector nucleating at an edge with its wavevector parallel to the edge. (c) The new wavevector nucleating at an edge with its wavevector perpendicular to the edge.
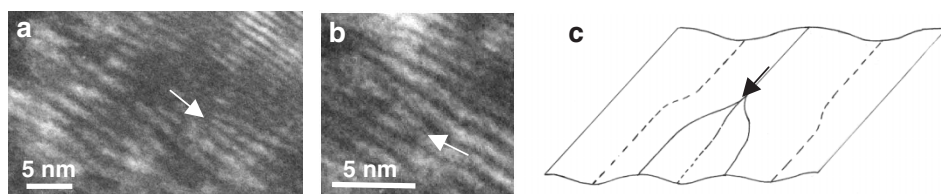
Figure 11. Dislocations in the structural modulation. (a) and (b) show faults reminiscent of edge dislocations in the structural modulation observed in $La_{0.5}Ca_{0.5}MnO_3$ at 90 K and (c) shows a schematic of this type of fault in three dimensions. Dotted lines show the position of minima in the wave and solid lines the position of maxima. A dislocation occurs where two waves of different wavelength meet. Arrows indicate the 'nodes' of the dislocations.

frequently observed in dark field images and figure 11 shows two examples together with a schematic representing this type of 'dislocation' in three dimensions. Such 'dislocations' seem to be intrinsic to the modulated structure since bright and dark field images from parent lattice reflections do not show dislocations or similar faults in the same areas.

5. Discussion and conclusions

The idea that the 'charge ordering' modulation should be composed of supercells which are an integer multiple of the undistorted unit cell is a direct result of assuming that the modulation is the result of a localisation of Mn^{3+} and Mn^{4+} ions. We have shown that the structural modulation need not be in registry with the parent lattice and it is therefore likely that the accompanying charge modulation is not in registry with the parent lattice as well. If this is the case, then individual manganese ions should adopt a range of valencies, not merely integer values. The possibilities go beyond this: it is not necessarily the manganese ions which have the mixed valency. Indeed, Hartree–Fock simulations which determine the charge distribution from the structure of the material suggest that it is the oxygen valency which varies [15]. Nor is it necessary that an entire electron be transferred during the charge ordering transition and valence bond sums by Daoud-Aladine *et al.* [16] suggest that it may in fact be as little as 1/100 of the electron charge.

The facts that the modulation need not be in registry with the parent lattice and also that the modulation wavevector need not be collinear with the $\mathbf{a}^*$ direction lead us to think that the modulation is weakly coupled to the parent lattice. We therefore consider it more likely that the structural distortion is the result of a charge density wave. The mechanism usually used to account for the occurrence of a charge density wave is Fermi surface nesting although other mechanisms have been suggested for different materials all of which are labelled as charge density wave systems [17, 18, 19]. We note that resistivity versus temperature curves for 'charge ordered' manganites do not show a metal–insulator transition but then neither do many curves for other charge density wave systems (see, for example, Fogle and Perlstein [20], Jiang *et al.* [21], Lue *et al.* [22], Naito and Tanaka [23], Rossnagel *et al.* [24]).

Our results suggest that the manganites may be pseudogap [25] materials where electrons are present at the Fermi level but are small in number, in agreement with observations made by optical spectroscopy for $La_{1-x}Ca_xMnO_3$, $0.5 < x < 0.67$ [26].

The 'charge ordering' modulation is not simply seen in the low temperature antiferromagnetic phase but has been observed at room temperature in $x = 0.52$ in this investigation and Zuo and Tao [27] have observed the same modulation in $x = 1/3$ both in the room temperature paramagnetic phase and at 114 K in the ferromagnetic phase. It has also been demonstrated that charge order can occur in both ferromagnetic and non-ferromagnetic regions of $La_{0.5}Ca_{0.5}MnO_3$ [28].

It is possible to explain these effects within the pseudogap model. The density of states at the Fermi energy is finite and a reduction in energy may occur by Fermi surface nesting and the formation of a charge density wave. Unless the nesting is perfect however, there will still be a finite density of states at the Fermi level. Thus, 'metallic' conductivity and the existence of a structural modulation are not mutually exclusive. It is simply that the stronger one is, the weaker the other.

The size of the pseudogap will be dependent on the materials from which the manganite is made. For $(La,Sr)MnO_3$ the paramagnetic phase is 'metallic' and therefore the pseudogap must be smaller than for $(La,Ca)MnO_3$. Following this argument, $(Pr,Ca)MnO_3$ has the largest pseudogap and this may explain why it does not show a metallic phase for $x < 1/2$.

The pseudogap explanation is similar to an alternative theory to double exchange and superexchange put forward by Ramakrishnan *et al.* [29]. In this model, electrons can be in either a localized polaronic state or a delocalized band and as composition and temperature changes, the number of electrons in each state and thus the character of the material changes. The essential difference between these models and more conventional explanations is that both localised and itinerant electrons are present in all compositions and at all temperatures and that the phase transitions observed in manganites can be explained by small changes in the proportion of each.

Acknowledgements

References

[1] S.-W. Cheong and H.Y. Hwang, in *Colossal Magnetoresistive Oxides*, edited by Y. Tokura (Gordon and Breach, the Netherlands, 2000).
[2] A.P. Ramirez, P. Schiffer, S.-W. Cheong, C.H. Chen, W. Bao, T.T.M. Palstra, P.L. Gammel, D.J. Bishop, B. Zegarski, Phys. Rev. Lett. **76** 3188 (1996).
[3] P.G. Radaelli, D.E. Cox, M. Marezio, S.-W. Cheong, Phys. Rev. B **55** 3015 (1997).
[4] P. Bak, Rep. Prog. Phys. **45** 587 (1982).
[5] G. Shao, Intermetallics **10** 493 (2002).
[6] S. Mori, C.H. Chen, S.-W. Cheong, Nature **392** 473 (1998).
[7] C.H. Chen, S. Mori, S.-W. Cheong, J. Phys. IV France **9** 307 (1999).
[8] C. Giacovazzo, H.L. Monaco, G. Artioli, D. Viterbo, G. Ferraris, G. Gilli, G. Zanotti, M. Catti, *Fundamentals of Crystallography*, second edn (Oxford University Press, Oxford, 2002) p. 244.
[9] D.B. Williams and C.B. Carter, *Transmission Electron Microscopy* (Plenum Press, New York, 1996) pp. 303–318.
[10] C.H. Chen, S. Mori, S.-W. Cheong, Phys. Rev. Lett. **83** 23 4792 (1999).
[11] R.H. Wang, J.I. Gui, Y.M. Zhu, A.R. Moodenbaugh, Phys. Rev. B **63** 14 144106 (2001).

[12] C.H. Chen and S.-W. Cheong, Phys. Rev. Lett. **76** 4042 (1996).
[13] J.C. Loudon, PhD thesis, Cambridge University (2004).
[14] D.J. Eaglesham, D. Bird, R.L. Withers, J.W. Steeds, J. Phys. C **18** 1 (1985).
[15] V. Ferrari, M. Towler, P.B. Littlewood, Phys. Rev. Lett. **91** 227202 (2003).
[16] A. Daoud-Aladine, J. Rodríguez-Carvajal, L. Pinsard-Gaudart, M.T. Fernández-Díaz, A. Revcolevschi, Phys. Rev. Lett. **89** 097205 (2002).
[17] R.M. White and G. Lucovsky, Il Nuovo Cimento **38** 280 (1977).
[18] J.A. Wilson, Solid St. Commun. **22** 551 (1977).
[19] H.P. Hughes, J. Phys. C **10** L319 (1977).
[20] W. Fogle and J.H. Perlstein, Phys. Rev. B **6** 1402 (1972).
[21] Y. Jiang, Z.-G. Liu, X.-X. Qu, X.J. Zhang, X.Y. Zhou, J. Phys. condensed Matter **3** 7129 (1991).
[22] C.S. Lue, Y.-K. Kuo, F.H. Hsu, H.H. Li, H.D. Yang, P.S. Fodor, L.E. Wenger, Phys. Rev. B **66** 033101 (2002).
[23] M. Naito and S. Tanaka, J. Phys. Soc. Japan **51** 219 (1982).
[24] K. Rossnagel, L. Kipp, M. Skibowski, Phys. Rev. B **65** 235101 (2002).
[25] N.F. Mott, Phil. Mag. **13** 989 (1966).
[26] K.H. Kim, S. Lee, T.W. Noh, S.-W. Cheong, Phys. Rev. Lett. **88** 167204 (2002).
[27] J.M. Zuo and J. Tao, Phys. Rev. B **63** 060407 (2001).
[28] J.C. Loudon, N.D. Mathur, P.A. Midgley, Nature **420** 797 (2002).
[29] T.V. Ramakrishnan, H.R. Krishnamurthy, S.R. Hassan, G. Venketeswara Pai, cond-mat/0308396 (2003).